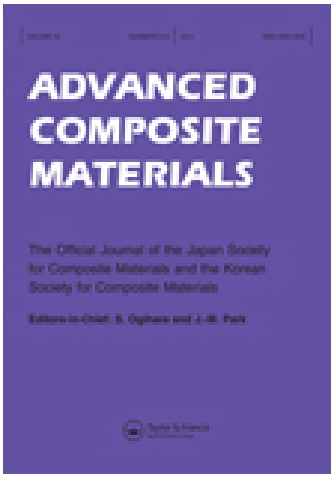

Advanced Composite Materials
Publication details, including instructions for authors and subscription information:
http://www.tandfonline.com/loi/tacm20

Recent efforts toward modeling interactions of matrix cracks and delaminations: an integrated XFEM-CE approach

T.E. Tay[a], X.S. Sun[a] & V.B.C. Tan[a]
[a] Department of Mechanical Engineering, National University of Singapore, 9 Engineering Drive 1, Singapore 117576, Singapore
Published online: 12 May 2014.

To cite this article: T.E. Tay, X.S. Sun & V.B.C. Tan (2014) Recent efforts toward modeling interactions of matrix cracks and delaminations: an integrated XFEM-CE approach, Advanced Composite Materials, 23:5-6, 391-408, DOI: 10.1080/09243046.2014.915092

To link to this article: http://dx.doi.org/10.1080/09243046.2014.915092

Advanced Composite Materials, 2014
Vol. 23, Nos. 5–6, 391–408, http://dx.doi.org/10.1080/09243046.2014.915092

Recent efforts toward modeling interactions of matrix cracks and delaminations: an integrated XFEM-CE approach

T.E. Tay*, X.S. Sun and V.B.C. Tan

Department of Mechanical Engineering, National University of Singapore, 9 Engineering Drive 1, Singapore 117576, Singapore

(*Received 21 November 2013; accepted 26 March 2014*)

This paper presents a novel integrated approach using the extended finite element method (XFEM) and cohesive elements (CEs) for modeling three-dimensional (3D) delaminations, matrix cracks, and their interactions in progressive failure of composite laminates. In the proposed XFEM-CE approach, the matrix cracks are explicitly modeled by the XFEM through nodal enrichment and element partition, and the inter-ply delaminations are modeled by cohesive elements through traction–separation law. An XFEM-based cohesive element enrichment scheme is developed in order to properly model the interactions between the delaminations and matrix cracks. It is critical to enrich the cohesive elements at the local juncture where cracks meet, in order to obtain the correct crack path interactions. Examples are presented for failure analysis of double-cantilever-beam and end-notch-flexure laminates with different layups. The results show strong explicit matrix crack–delamination interactions in these laminates. This work presents another significant development of a computational platform for realistic modeling of progressive damage in composites.

Keywords: composite laminate; matrix crack; delamination; XFEM; cohesive element; XFEM-CE approach

1. Introduction

Accurate and efficient computational modeling of progressive failure in composite structures with due consideration of the underlying physics is still challenging because of the various complex failure mechanisms such as delamination, splitting, matrix cracking, debonding, local buckling, and so on.[1,2] These failure mechanisms occur simultaneously but across vastly different length scales. For example, while matrix cracks may extend several millimeters or centimeters in the plane of the laminate, they are usually constrained by surrounding plies and are fractions of a millimeter in the thickness direction. Similarly, delaminations may extend several centimeters, but their interactions with smaller matrix cracks have profound effects on subsequent damage propagation. While the finite element method (FEM) is the most widely used computational method for failure analysis of composites, careful mesh design and appropriate failure theories are usually required, especially in progressive failure analysis. Special computational schemes such as the extended finite element method (XFEM) for modeling general crack propagation through local nodal enrichments without having to

*Corresponding author. Email: mpetayte@nus.edu.sg

resort to substantial remeshing have been developed.[3–5] Although the XFEM has been applied to interfacial damage and delamination analysis in composites,[6,7] the cohesive element (CE) method is currently more commonly used for delamination problems [2,8] because it is available in many commercial FE softwares and, therefore, more convenient to users. Recently, some nodal enrichment schemes have also been adopted in cohesive elements to more accurately model cohesive crack and delamination problems.[9–12] These enrichment schemes, however, are specifically designed for cohesive elements based on some special enrichment functions such as isotropic analytical functions,[9] solutions of isotropic beams on elastic foundation [10,11], and piecewise linear functions.[12] They are only suitable for modeling single delamination-type problems and interactions between delamination and crack kinking are generally not considered. In order to model crack bifurcation problems, an augmented cohesive zone model was proposed in an augmented finite element method framework.[13] In this model, separable mathematical elements instead of nodal enrichment were adopted to simulate delaminaton and cracks. This method was used to model two-dimensional (2D) delamination jumps in a cross-ply single-cantilever beam.

Recently, the authors have developed an integrated XFEM-CE approach for modeling matrix cracks and delamination interactions in cross-ply and angled-ply double-cantilever-beam laminates.[14,15] This paper extends the previous work and presents an integrated XFEM-CE approach for modeling 3D complex failures in general composite laminates. This approach combines XFEM and cohesive elements and adopts a consistent nodal enrichment scheme for both solid elements and cohesive elements. Delamination, matrix cracks, and their interactions are modeled explicitly and seamlessly by cohesive elements and solid elements through nodal enrichment within the XFEM framework. Examples on failure analysis of double-cantilever-beam and end-notch-flexure laminates with different layups are presented to demonstrate the application of the proposed XFEM-CE approach.

2. The XFEM-CE approach for modeling complex failures in composite laminates

The XFEM-CE approach is based on the XFEM framework to model multiple failures in composites using both solid and cohesive elements. The XFEM is used to model arbitrary matrix cracks through nodal enrichment and element partition. The cohesive elements are used to model interface behaviors and delamination through the traction–separation law. For the interaction between the interlayer delamination and matrix cracks, enriched cohesive elements are adopted to account for the interaction. This approach is implemented with an in-house finite element analysis (FEA) code written with FORTRAN. The procedure of the FEA using the proposed approach is illustrated in Figure 1, where the implicit method is used to obtain the solutions of the nonlinear finite element equations.

2.1. Crack modeling by the XFEM

2.1.1. Basic equations in the XFEM

In the XFEM, nodal enrichment with the same shape functions of standard elements is used to implicitly model strong (cracks) and weak (material interfaces) discontinuities. The enrichment functions may vary with the discontinuity types. Two kinds of enrichment functions, namely the Heaviside function and the tip enrichment functions,

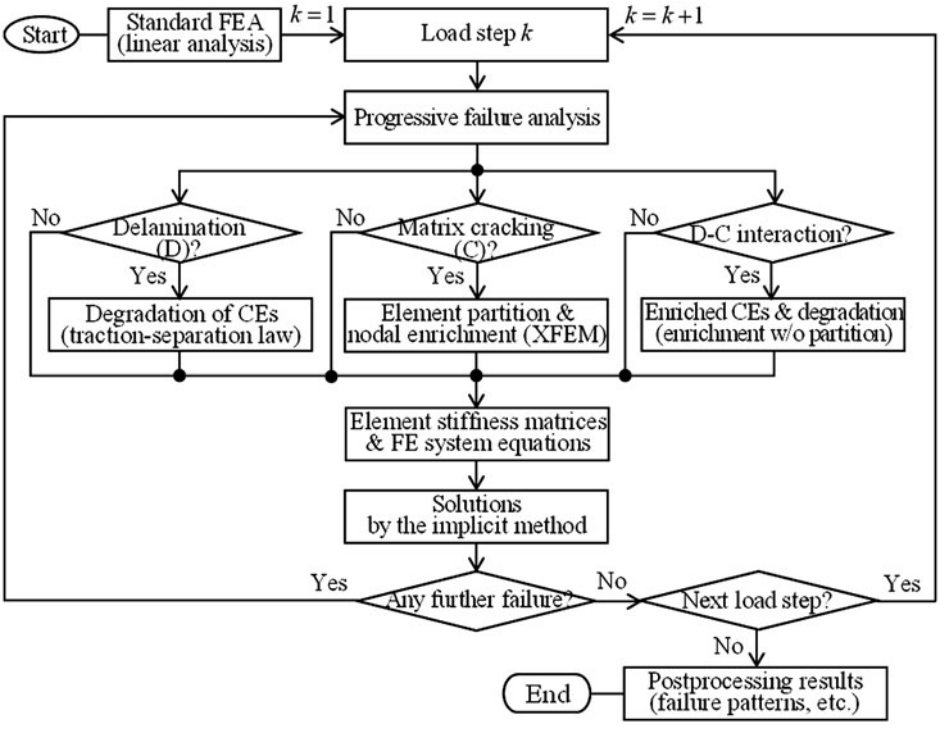

Figure 1. Flowchart of implementing the integrated XFEM-CE approach.

are usually used for crack-type problems. The Heaviside function, representing the displacement discontinuity across the crack surface, is typically used in fully cracked elements, where the crack tip or front is always located at element edges. The tip enrichment functions are a series of bases of asymptotic expansions of displacement fields around the crack tip. These functions are used in partially cracked elements in order to obtain more accurate solutions around the crack tip or front, where the crack tip or front is located within elements. However, these asymptotic expansions are difficult to obtain for some cases such as 3D cracks in anisotropic materials. An approach to circumvent this issue in applying XFEM to the 3D crack problems of composite materials is to model the cracks with only fully cracked elements and reasonably small element sizes near the crack tip, where only the Heaviside function is used for nodal enrichment.

In this paper, multiple cracks are allowed in the modeling, but it is assumed that a node support or an element can be cut by only one crack and the crack surface remains plane within the element. Crack kinking is allowed but only at element edges. With the fully cracked-element scheme in XFEM, the displacement approximation $\boldsymbol{u}(\boldsymbol{x})$ in an element can be written as follows:

$$\boldsymbol{u}(\boldsymbol{x}) = \sum_{i=1}^{n^e} \boldsymbol{N}_i(\boldsymbol{x}) \cdot (\boldsymbol{u}_i^e + H(\boldsymbol{x})\boldsymbol{a}_i^e) \tag{1}$$

where $\boldsymbol{N}_i(\boldsymbol{x})$ is the shape function matrix at node i and n^e is the number of nodes in the element; $\boldsymbol{u}_i^e$ and $\boldsymbol{a}_i^e$ are the standard and additional (enriched) degree of freedoms (DOFs) at node i of the element, respectively; $H(\boldsymbol{x})$ is the Heaviside function.

For any point $\boldsymbol{x}$ in an element with enriched nodes, the Heaviside function $H(\boldsymbol{x})$ can be determined by position of the point $\boldsymbol{x}$ to the crack surface as follows:

$$H(\boldsymbol{x}) = \begin{cases} \frac{\boldsymbol{n}_c \cdot (\boldsymbol{x} - \boldsymbol{x}_c)}{|\boldsymbol{n}_c \cdot (\boldsymbol{x} - \boldsymbol{x}_c)|}, & \boldsymbol{n}_c \cdot (\boldsymbol{x} - \boldsymbol{x}_c) \neq 0 \\ 0, & \boldsymbol{n}_c \cdot (\boldsymbol{x} - \boldsymbol{x}_c) = 0 \end{cases} \tag{2}$$

where $\boldsymbol{x}_c$ and $\boldsymbol{n}_c$ are, respectively, a given point and the normal defining the crack surface corresponding to the element.

From Equation (2), it can be seen that the values of $H(\boldsymbol{x}) = 1, -1, 0$ correspond to the point $\boldsymbol{x}$ above, below, and on the crack surface, respectively.

2.1.2. *Determination of nodal enrichment and element partition*

In modeling cracks with XFEM, only some nodes around the cracks need to be enriched. The enrichment at a node is determined by the rule that the node or its support is cut by cracks. In order to ensure displacement continuity around the crack tip or front, all nodes at element edges where the crack tip or front is located will not be enriched (Figure 2(a)). A subroutine in the in-house code is developed to determine the node list for enrichment and then automatically implement the partition of elements cut by cracks. This is illustrated with a simple 3D example in Figure 2.

Depending on the crack position and nodal enrichment, there are usually three categorizations of elements in XFEM: (1) standard elements (continuous and un-enriched), (2) cracked elements (discontinuous and enriched) which are cut by cracks into two parts, and (3) affected elements (continuous and enriched) which are not cut by any crack but include at least one enriched node, as shown in Figure 2(a). For the standard and affected elements, regular numerical integration methods (e.g. the Gaussian quadrature method) can be used to calculate the element stiffness. For the cracked elements, however, special integration schemes are used because of the discontinuity.[4] This paper adopts an element-partitioning method for the numerical integration of cracked elements. The element partition is based on the triangulation of 2D polygons or tetrahedralization of 3D polyhedrons. An element cut by a crack is divided into two parts above and below the crack plane, respectively, and each part is a simple 2D polygon or

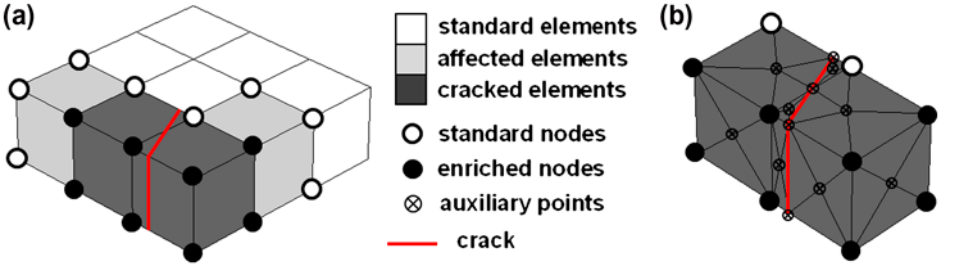

Figure 2. Nodal enrichment and element partition in XFEM: (a) finite elements with enriched nodes and (b) partitioned elements.

3D polyhedron. The 2D triangulation or 3D tetrahedralization is carried out for both parts by sequentially connecting the centroids and vertices of the polygons or polyhedrons through some elementary computational geometry techniques.[16] This partition procedure is automatically implemented with the developed subroutine, through which all cracked elements are partitioned into 2D triangular or 3D tetrahedral sub-elements as shown in Figure 2(b).

Then the numerical integration of the cracked elements is implemented in the sub-elements through regular numerical integration methods (e.g. the Hammer quadrature method). Auxiliary points are generated to form the sub-elements in partitioning cracked elements (Figure 2(b)). It should be noted that these auxiliary points are simply used in the numerical integration of the cracked elements but not involved in the node-based system equations. In other words, the integration of the cracked elements is implemented in the sub-elements but the element stiffness assembly is still based on the nodes of the cracked elements.[7] The element stiffness assembly in XFEM follows the same procedure as that in standard FEM, except that the size of the stiffness matrix of an element with enriched nodes is expanded due to the additional degrees of freedom (DOFs).[3,4]

2.1.3. *Failure criterion for solid elements*

With the nodal enrichment and element partition, arbitrary cracks can be modeled explicitly in XFEM. A failure criterion is required to determine crack initiation in an element. There have been many failure criteria for composite materials in the literature.[17,18] For simplicity and illustrative purposes, but without loss of generality, the maximum stress criterion is used in this paper to determine the failure initiation of solid elements. For composite materials with different tensile and compressive strengths, the maximum stress criterion can be expressed as follows:

$$f_F = \max\left\{\frac{\sigma_i^2}{S_i^T S_i^C} + \left(\frac{1}{S_i^T} - \frac{1}{S_i^C}\right)\sigma_i\right\} \leqslant 1 \tag{3}$$

where f_F is the failure index; σ_i $(i = 1, 2, \ldots, 6)$. are stress components in the material coordinate system (local stress components); S_i^T and S_i^C are the tensile and compressive strengths in the direction i, respectively.

Once the failure index $f_F \geqslant 1$ in a solid element, failure initiation is detected and the element will be cut by a crack plane though its centroid. In a non-interactive failure criterion such as the maximum stress criterion, if the failure is caused by normal stress, the normal of the crack plane ($\boldsymbol{n}_c$) is aligned with the direction of the maximum normal failure stress $\sigma_{\max}^f$; otherwise if the failure is caused by shear stress, the normal of the crack plane is perpendicular to the direction of the maximum shear failure stress $\tau_{\max}^f$, as shown in Figure 3(a). It should be noted that the normal and shear failure stresses ($\sigma_{\max}^f$ or $\tau_{\max}^f$) may not coincide with the maximum values of the stress components due to the directional strength properties of the composite material. For interactive failure criteria, however, the orientation of the crack plane (or fracture angle) is generally determined from fracture stress state in the element and failure conditions of the corresponding interactive criterion. Once a crack initiates in a solid element, it may propagate to an adjacent solid element due to stress concentration around the crack tip or front. For simplicity, it is assumed that the new crack in the adjacent element is

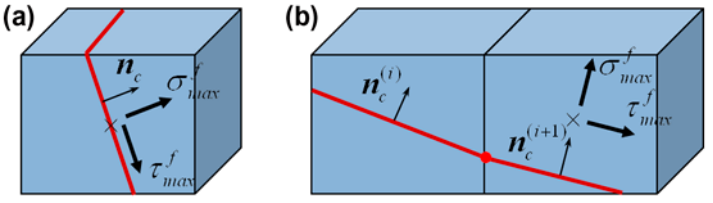

Figure 3. Orientation of the crack plane in a solid element: (a) failure initiation and (b) failure propagation to an adjacent element.

connected to the initial crack, as shown in Figure 3(b), and the orientation of the new crack plane ($\boldsymbol{n}_c^{(i+1)}$) is determined by the maximum normal or shear failure stress in the adjacent element. The failure of a solid element is evaluated at an integration point of the element with the failure criterion. The crack plane, however, may not necessarily pass through the integration point. The position of the crack plane in a failed solid element depends on the previous crack tip or front as shown in Figure 3(b). The element cut by a crack is assumed fully separated. Then the nodal enrichment is activated and element partition is implemented. The XFEM-based element partition is performed only for solid elements; a different scheme is used to treat failure in cohesive elements, as described below.

2.2. *Delamination modeling by cohesive elements*

2.2.1. *Cohesive elements and failure criteria*

In a cohesive finite element, the stiffness $\boldsymbol{K}_h^e$ can be written as follows:

$$\boldsymbol{K}_h^e = \int_\Omega \boldsymbol{N}_u^T \boldsymbol{D}_h \boldsymbol{N}_u d\Omega \tag{4}$$

where Ω corresponds to the domain of the mid-plane of the cohesive element; $\boldsymbol{D}_h$ is the material stiffness matrix of the cohesive element; and $\boldsymbol{N}_u$ is the deformation matrix of the cohesive element and for 3D problem

$$\boldsymbol{N}_u = [\boldsymbol{N}_h \quad -\boldsymbol{N}_h] \tag{5}$$

$$\boldsymbol{N}_h = [\boldsymbol{N}_1 \quad \boldsymbol{N}_2 \quad \ldots \quad \boldsymbol{N}_{n_h/2}] \tag{6}$$

$$\boldsymbol{N}_i = N_i \boldsymbol{I}, \quad i = 1, 2, \ldots, n_h/2 \tag{7}$$

where $\boldsymbol{I}$ is the unit matrix; N_i is the value of shape function at node i, and n_h is the total number of nodes in the cohesive element.

In the progressive failure analysis with cohesive elements, traction-based and energy-based criteria are adopted to determine the failure initiation and evolution of cohesive elements, respectively. These two criteria can be written as follows:

$$\left(\frac{\langle t_n \rangle}{S_n}\right)^2 + \left(\frac{t_s}{S_s}\right)^2 + \left(\frac{t_t}{S_t}\right)^2 \leqslant 1 \tag{8}$$

$$G_T \leqslant G_{Tc} \tag{9}$$

where t_n, t_s, and t_t are the normal and two shear tractions, respectively, and $\langle\rangle$ denotes the positive value; S_n, S_s, and S_t are cohesive strengths along the normal and two shear directions, respectively; G_T and G_{Tc} are the total deformation energy and equivalent critical energy of a cohesive element, respectively.

The total deformation energy of a cohesive element is a summation of the deformation energies along the normal and two shear directions in the element, i.e.:

$$G_T = G_n + G_s + G_t \tag{10}$$

The equivalent critical energy of a cohesive element can be calculated from a specified failure evolution law, such as the BK law or power law. In this paper, the power law is adopted and G_{Tc} can be written as follows:

$$G_{Tc} = \left(\frac{m_n}{G_{\mathrm{Ic}}} + \frac{m_s}{G_{\mathrm{IIc}}} + \frac{m_t}{G_{\mathrm{IIIc}}}\right)^{-1} \tag{11}$$

where G_{Ic}, G_{IIc}, and G_{IIIc} are the critical fracture energies corresponding to the three fracture modes; m_n, m_s, and m_t are three energy-based mode ratios which are calculated from initial elastic deformations and assumed constants throughout the failure progression in the cohesive element.

2.2.2. *A zig-zag evolution model for progressive failure of cohesive elements*

The progressive failure of cohesive elements is usually modeled through a traction–separation law. The models of traction–separation law may have different formulations such as linear, trapezoidal, and exponential models.[19] In these models, the stiffness of cohesive elements becomes variable after failure initiation, which may result in convergence problems or long-time iterations for convergence during the numerical simulation. This paper employs a zig-zag evolution model which is based on the linear model of traction–separation law. In this model, the stiffness of cohesive elements is constant within each load increment and, therefore, fewer iterations are required in the computation, which can improve the computational time and circumvent the potential convergence problems.

For mixed-mode deformation of cohesive elements, the equivalent traction t, and equivalent separation δ are defined as follows:

$$\begin{cases} \delta = \sqrt{\langle \delta_n \rangle^2 + \delta_s^2 + \delta_t^2} \\ t = \sqrt{\langle t_n \rangle^2 + t_s^2 + t_t^2} \end{cases} \tag{12}$$

where δ_n, δ_s, and δ_t are the normal and two shear separations, respectively.

Based on the linear traction–separation law as shown in Figure 4, the separations corresponding to failure initiation and total failure of a cohesive element, δ_0 and δ_f, are, respectively, calculated as follows:

$$\begin{cases} \delta_0 = t_0/E_0 \\ \delta_f = 2G_{Tc}/t_0 \end{cases} \tag{13}$$

where E_0 is the initial elastic modulus of the cohesive element; t_0 is the maximum equivalent traction determined from Equations (8) and (12); and the total equivalent critical energy G_{Tc} is determined from Equation (11).

In the traction–separation plotting as shown in Figure 4, the zig-zag evolution model consists of a number of zig-zags instead of linear segment in the linear evolution mode. For the kth zig-zag, the separation increment $\Delta\delta_k$ is divided into two parts $\Delta\delta_k^0$ and $\Delta\delta_k^a$, i.e.:

$$\begin{cases} \Delta\delta_k = \delta_k - \delta_{k-1} = \Delta\delta_k^0 + \Delta\delta_k^a \\ \Delta\delta_k^0 = \delta_k^a - \delta_{k-1} \\ \Delta\delta_k^a = \delta_k - \delta_k^a \end{cases} \tag{14}$$

where δ_{k-1} and δ_k are the separations after $k-1$ and k zig-zags, respectively; and δ_k^a is an intermediate value between δ_{k-1} and δ_k, which needs to be determined in the kth zig-zag.

In Figure 4, two energies ΔG_k^+ and ΔG_k^- are defined with $\Delta\delta_k^0$ and $\Delta\delta_k^a$ as follows:

$$\begin{cases} \Delta G_k^+ = \dfrac{1}{2}\Delta\delta_k^0(t_k^e - t_k^a) \\ \Delta G_k^- = \dfrac{1}{2}\Delta\delta_k^a(t_k^a - t_k') \end{cases} \tag{15}$$

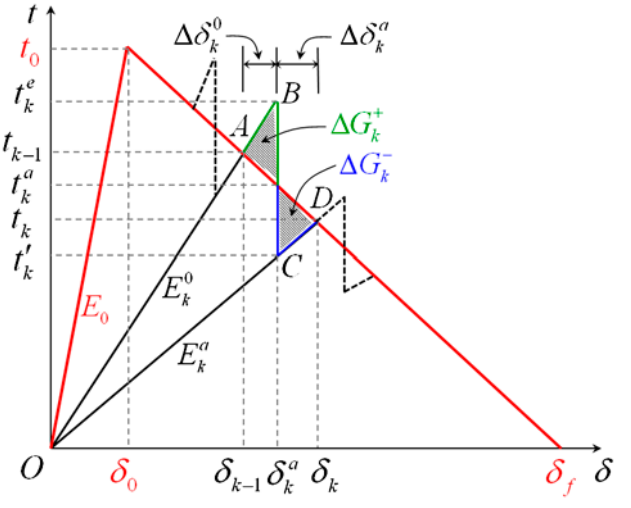

Figure 4. Zig-zag evolution model based on linear traction–separation law.

where the tractions t_k^e, t_k^a, and t_k' can be calculated from t_0 as follows:

$$t_k^e = E_k^0 \delta_k^a = t_0 \cdot \frac{\delta_k^a(\delta_f - \delta_{k-1})}{\delta_{k-1}(\delta_f - \delta_0)} \tag{16}$$

$$t_k^a = t_0 \cdot \frac{\delta_f - \delta_k^a}{\delta_f - \delta_0} \tag{17}$$

$$t_k' = E_k^a \delta_k^a = t_0 \cdot \frac{\delta_k^a(\delta_f - \delta_k)}{\delta_k(\delta_f - \delta_0)} \tag{18}$$

In the zig-zag evolution model (segment *ABCD*) as shown in Figure 4, energy balance requires $\Delta G_k^+ = \Delta G_k^-$, where the dissipated energy equals to that in the linear evolution model (segment *AD*). With $\Delta G_k^+ = \Delta G_k^-$, the separation δ_k^a can be determined as follows:

$$\delta_k^a = \sqrt{\delta_{k-1}\delta_k} \tag{19}$$

By defining a separation ratio $c_k = \Delta\delta_k^0/\delta_{k-1}$, the separations δ_k^a, δ_k, $\Delta\delta_k^a$, and $\Delta\delta_k$ are rewritten as follows:

$$\begin{cases} \delta_k^a = (1 + c_k)\delta_{k-1} \\ \delta_k = (1 + c_k)^2 \delta_{k-1} \end{cases} \tag{20}$$

$$\begin{cases} \Delta\delta_k^a = c_k \delta_k^a = (c_k + c_k^2)\delta_{k-1} \\ \Delta\delta_k = (2c_k + c_k^2)\delta_{k-1} \end{cases} \tag{21}$$

From Equations (16)–(21), once one of the values of c_k or $\Delta\delta_k$ is known, all other parameters required to define the kth zig-zag can be determined from δ_{k-1}, δ_0, δ_f, and t_0. In the progressive analysis, $\Delta\delta_k$ can be determined from a pre-defined number of zig-zags, N_z, i.e.:

$$\Delta\delta_k = (\delta_f - \delta_0)/N_z \tag{22}$$

Then the parameters defining all the zig-zags ($k = 1, 2, \ldots, N_z$) can be determined from Equations (16)–(21). As shown in Figure 4, two stiffness parameters E_k^0 and E_k^a in each zig-zag are used and they are determined as follows:

$$E_k^0 = E_{k-1}^a \tag{23}$$

$$E_k^a = (1 - d_k)\, E_0 = \frac{t_0}{\delta_k} \cdot \frac{\delta_f - \delta_k}{\delta_f - \delta_0} \tag{24}$$

where d_k is a degradation factor in the kth zig-zag and can be written as follows:

$$d_k = \frac{\delta_f}{\delta_k} \cdot \frac{\delta_k - \delta_0}{\delta_f - \delta_0} \tag{25}$$

with the initial conditions $E_1^0 = E_0^a = E_0$ or $d_0 = 0$.

It can be seen that E_k^0 and E_k^a are constant in $\Delta\delta_k^0$ and $\Delta\delta_k^a$, respectively. Piece-wise constant stiffness is used in the zig-zag model instead of the variable stiffness in the linear model. From Equation (22), the values of $\Delta\delta_k$ (also $\Delta\delta_k^0$ and $\Delta\delta_k^a$) will increase with a smaller value of N_z. Therefore, the number of iterations for obtaining the nonlinear solutions of cohesive elements will become fewer than that for the linear model since E_k^0 and E_k^a are constant in the increment for the zig-zag model.

2.3. *Delamination–crack interaction modeling by enriched cohesive elements*

When an XFEM-based matrix crack encounters a cohesive element at an interface between two plies, two different failure modes interact. In this paper, the cohesive elements connecting the matrix crack are not partitioned but enriched to account for the interaction, as shown in Figure 5.

From Equations (1) and (5)–(7), for a general XFEM-based enriched cohesive element, the deformation matrix corresponding to the enrichment can be formulated as follows:

$$\boldsymbol{N}_a = H(\boldsymbol{x})\boldsymbol{N}_u \tag{26}$$

With the normal and enriched deformation matrices in Equations (5) and (26), the element stiffness for an enriched cohesive element can be formulated as follows:

$$\boldsymbol{K}_h^e = \begin{bmatrix} \boldsymbol{K}_{uu}^e & \boldsymbol{K}_{ua}^e \\ (\boldsymbol{K}_{ua}^e)^{\mathrm{T}} & \boldsymbol{K}_{aa}^e \end{bmatrix} \tag{27}$$

and

$$\boldsymbol{K}_{\alpha\beta}^e = \int_\Omega \boldsymbol{N}_\alpha^T \boldsymbol{D}_h \boldsymbol{N}_\beta d\Omega \tag{28}$$

where the subscripts α and β take the symbols of u or a, and $\boldsymbol{K}_{\beta\alpha}^e = (\boldsymbol{K}_{\alpha\beta}^e)^{\mathrm{T}}$; and Ω is the domain of the mid-plane of the cohesive element.

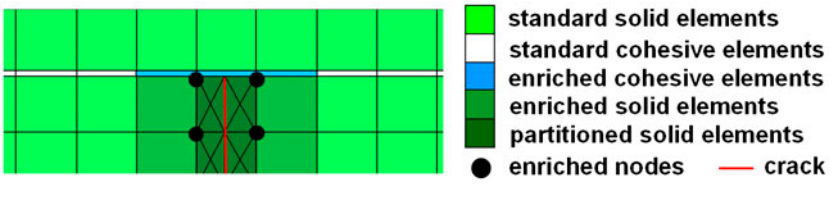

Figure 5. Interaction between cohesive elements and partitioned solid elements in XFEM.

In Equation (27), $\boldsymbol{K}^e_{uu}$ is the stiffness corresponding to the standard DOFs, which is the normal cohesive element stiffness (without enrichment) as shown in Equation (4); $\boldsymbol{K}^e_{aa}$ is the stiffness corresponding to the enriched DOFs, and $\boldsymbol{K}^e_{ua}$ is the stiffness corresponding to the interaction between the standard and enriched DOFs.

With Equation (27), the equilibrium equation of an enriched cohesive element can, therefore, be written as follows:

$$\begin{bmatrix} \boldsymbol{f}^e_u \\ \boldsymbol{f}^e_a \end{bmatrix} = \begin{bmatrix} \boldsymbol{K}^e_{uu} & \boldsymbol{K}^e_{ua} \\ (\boldsymbol{K}^e_{ua})^{\mathrm{T}} & \boldsymbol{K}^e_{aa} \end{bmatrix} \begin{bmatrix} \boldsymbol{u}^e \\ \boldsymbol{a}^e \end{bmatrix} \tag{29}$$

where $\boldsymbol{f}^e_u$ and $\boldsymbol{f}^e_a$ are the nodal force corresponding to the standard DOF $\boldsymbol{u}^e$ and additional DOF $\boldsymbol{a}^e$, respectively, in the cohesive element.

3. Examples and results

This section will demonstrate the application of the proposed XFEM-CE approach to failure analysis of composite laminates. Three examples, a cross-ply double-cantilever-beam (DCB), an angled-ply DCB, and an end-notched-flexure (ENF) laminated specimen, are presented to illustrate failure analysis with strong matrix crack–delamination interactions. In the numerical simulations, each ply is modeled with solid elements and each ply-interface is modeled with cohesive elements. The material of the laminates is assumed carbon/epoxy (AS4/3501-6); the properties are listed in Table 1. The elastic modulus of cohesive elements is assumed to be 4.0 GPa which is a typical value for the modulus of epoxy resin. The cohesive strengths and fracture energies for three failure modes are listed in Table 2.

3.1. *Failure analysis of a cross-ply DCB laminate*

A composite laminate with layup $[0/90]_s$ loaded as a double-cantilever beam (DCB) is used to illustrate failure analysis with strong matrix crack–delamination interactions in this example. The cross-ply laminate has a length $L = 125$ mm and width $W = 20$ mm; each ply and cohesive layer thicknesses are 1 and 0.005 mm, respectively. The 0- or fiber direction is aligned with the length direction (X-axis) of the laminate. The top 0/90 and bottom 90/0 interfaces are modeled with cohesive elements. A pre-existing interfacial crack is located at one end part of the top 0/90 interface, with the initial length $c_0 = 5$ mm and throughout the laminate width, as shown in Figure 6. The initial delamination crack front is a straight line perpendicular to the fiber direction in the top 0^o ply. Out-of-plane tensile loads are applied on both top and bottom surfaces of the laminate near the end with the pre-existing interfacial crack, while the other end of the laminate is fixed.

The FE model of the cross-ply laminate is built with 8-node hexahedral solid elements for four plies and 8-node hexahedral cohesive elements for the two interfaces between 0^o and 90^o plies, with one element per ply in the thickness direction. The cohesive elements share nodes with the solid elements in the adjacent plies, as shown in Figure 6.

The simulation results of delamination propagation and matrix cracking in the cross-ply laminate by the XFEM-CE approach are illustrated in Figure 7. With increasing applied load, the delamination propagates along the top 0/90 interface, and the

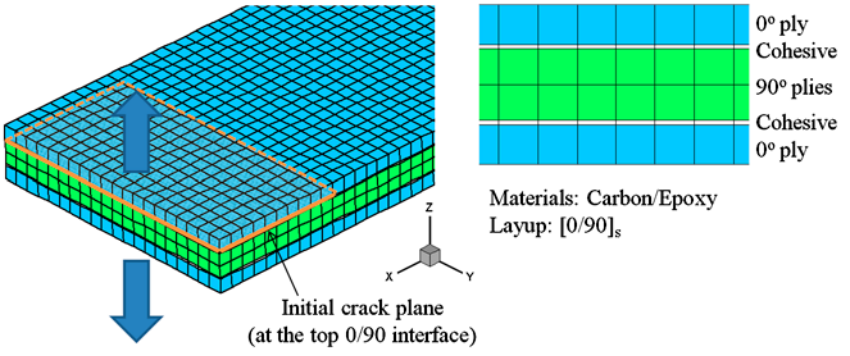

Figure 6. FE model of the DCB laminate: (a) mesh and (b) layup.

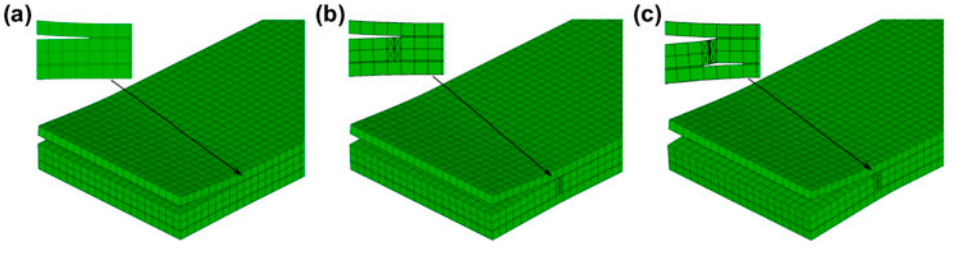

Figure 7. Failure progression and patterns: (a) delamination propagation at the top 0/90 interface, (b) matrix cracking in the 90° plies, and (c) delamination propagation at the bottom 90/0 interface.

delamination front is nearly parallel with the fiber direction in the 90° plies, as shown in Figure 7(a). After the delamination propagation length is about $\Delta c = 5$ mm, the maximum stress in the transverse direction of the 90° plies reaches the ply transverse strength, and the matrix crack automatically appears, which is modeled by the XFEM through nodal enrichment and element partition, as shown in Figure 7(b).

Because the strength in the transverse direction is much lower than that in the longitudinal direction, the matrix cracks in the 90° plies appear only after a short delamination at the top 0/90 interface, and the crack extends through the thickness of the 90° plies. Upon reaching the bottom 90/0 interface, the crack is temporarily arrested, before another delamination appears and propagates along the bottom 90/0 interface as shown in Figure 7(c).

3.2. *Failure analysis of an angled-ply DCB laminate*

This next example demonstrates the application of the proposed XFEM-CE approach to failure analysis of an angled-ply laminate with layup $[0/45]_s$ loaded as a DCB. The geometry and FE model are same as those in the previous example in Section 3.1 (Figure 6), except that the 90° plies are replaced with 45° plies and the initial length of the delamination is $c_0 = 10$ mm at the top 0/45 interface throughout the laminate width.

The failure progression and patterns are illustrated in Figure 8. The delamination at the top 0/45 interface propagates first, and the delamination front is similarly a straight line as its initial shape (Figure 8(a,b)). After the delamination propagates past a certain length, a matrix crack initiates at one edge in the 45° plies (Figure 8(b)). It quickly propagates throughout the thickness and width of the 45° plies (Figure 8(c)). Shortly after the crack in the 45° plies has reached the other edge (Figure 8(d)), another delamination (represented by the region colored red) initiates and propagates at the bottom 45/0 interface. This second delamination initiates at the edge opposite to that where the matrix crack initiates and then propagates throughout the width of the laminate (Figure 8(e,f)). The first delamination at the top 0/45 interface continues to propagate toward the right.

Thereafter, the delamination at the bottom 45/0 interface further propagates along the length direction of the laminate as shown in Figure 9. The deformations of the laminate and the cracked 45° plies are shown in Figure 10, where the delaminations and the major crack are explicitly modeled by the failed cohesive elements and the partitioned solid elements, respectively.

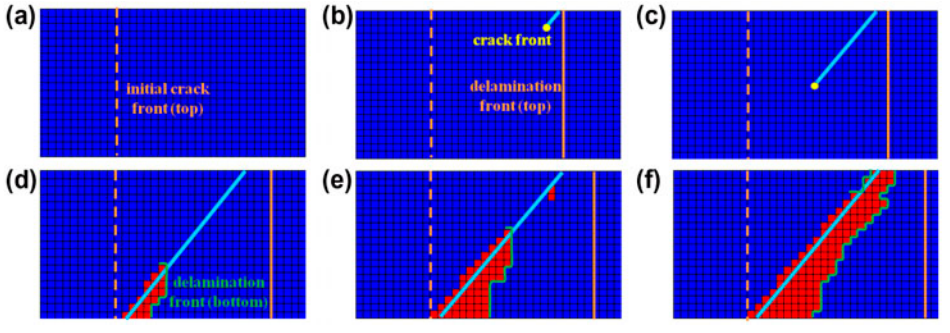

Figure 8. Failure progression and patterns: (a) initial crack at the top 0/45 interface, (b) delamination progression at the top 0/45 interface and matrix crack initiation, (c) matrix crack progression, (d) fully cracked 45° plies and delamination initiation at the bottom 45/0 interface, (e) delamination progression along the crack at the bottom 45/0 interface, and (f) delamination spreading throughout the width at the bottom 45/0 interface.

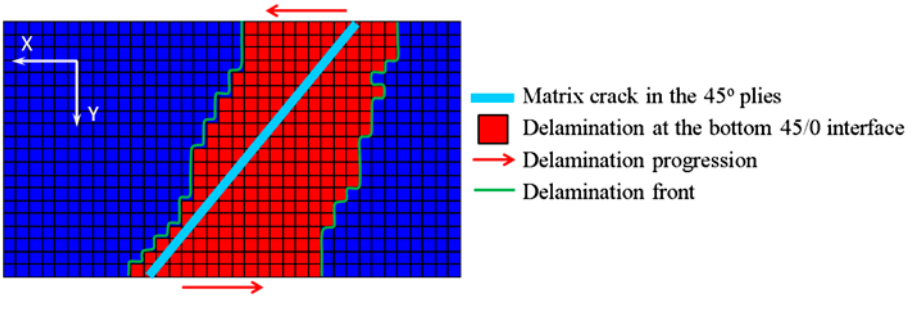

Figure 9. Delamination progression at the bottom 45/0 interface after spreading throughout the width.

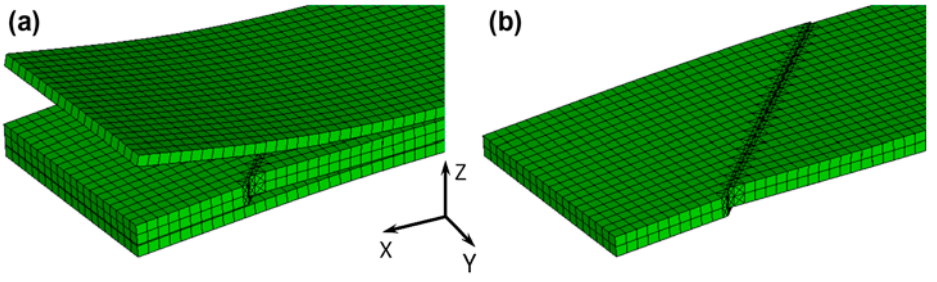

Figure 10. Deformations: (a) the laminate and (b) the 45° plies.

3.3. *Failure analysis of an ENF laminate*

The proposed XFEM-CE approach is applied to failure analysis of an ENF laminate (Figure 11). The layup of the ENF laminate is $[[0_2/90_2]_{2s}/[-45/90/45/0]_2]_s$, with length $L = 38.1$ mm, width $b = 16.5$ mm, total thickness $h = 6.2$ mm, and the initial delamination (pre-crack) length $a = 31.75$ mm. This specimen was originally used by Tao and Sun [22] to investigate delamination and crack jumps and interactions between plies.

In the FE model, the layup is reduced to $[0/-45/90/45/0]_s$, where the original cross plies are replaced with 0° plies in order to reduce computational time, as shown in Figure 12. The reduced layup does not alter the ply cracking and delamination events, which are similar to those in the original laminate. The FE model of the ENF laminate

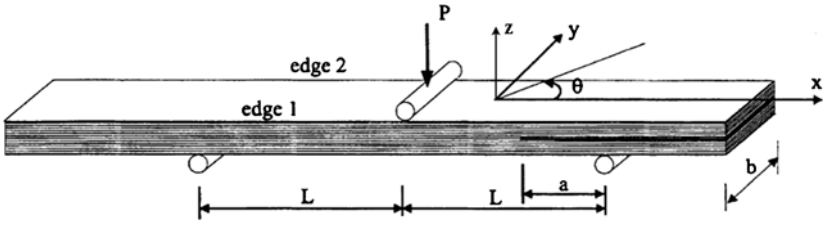

Figure 11. End-notch-flexure (ENF) specimen.[22]

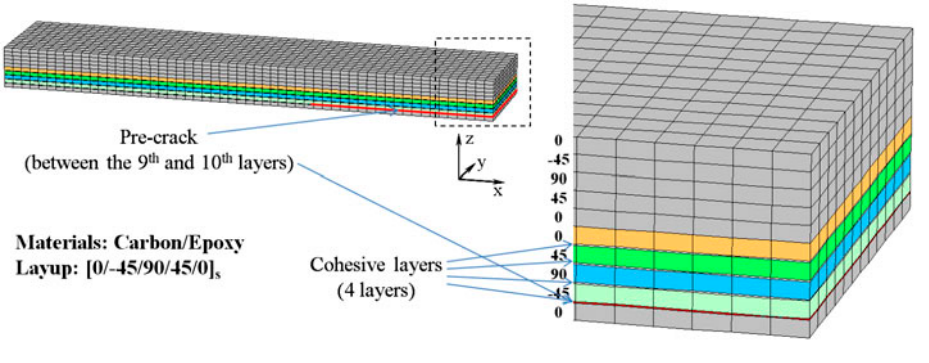

Figure 12. FE model of the ENF laminate.

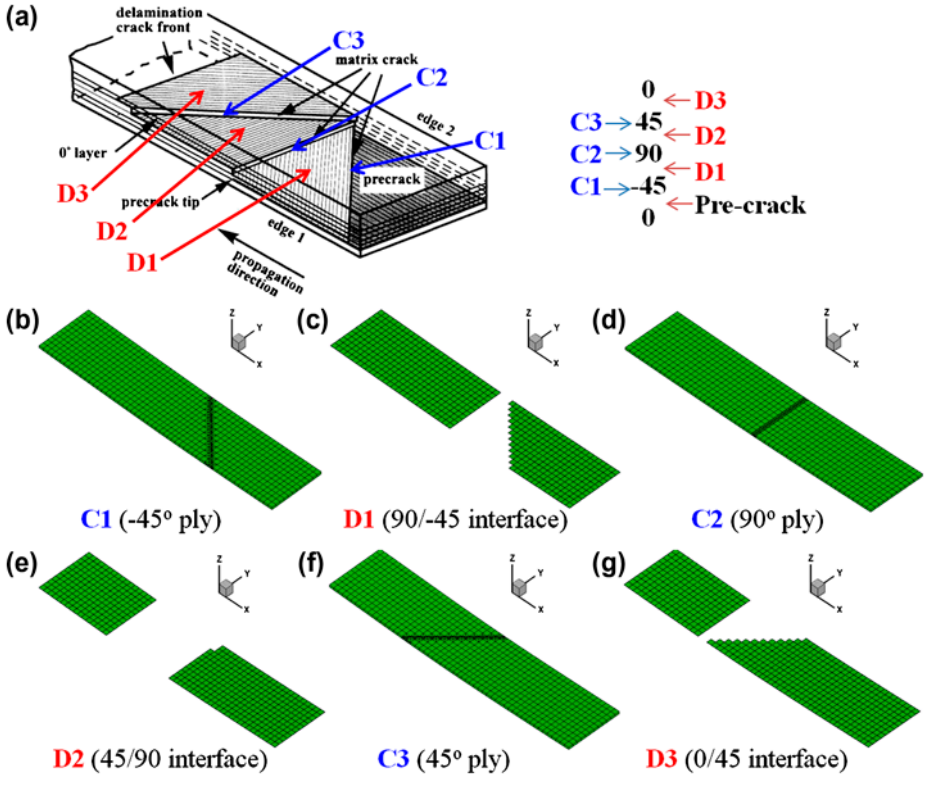

Figure 13. Failure patterns: (a) experimental results [22], (b) matrix crack in the −45° ply, (c) delamination at the 90/−45 interface, (d) matrix crack in the 90° ply, (e) delamination at the 45/90 interface, (f) matrix crack in the 45° ply, and (g) delamination at the 0/45 interface.

is built with 8-node hexahedral solid elements for plies and 8-node hexahedral cohesive elements for interfaces between plies, with one element in the thickness per ply. Only four interfaces below the symmetrical plane of the laminate are modeled with cohesive elements (Figure 12). The cohesive elements share nodes with the solid elements in the

Table 1. Material properties of AS4/3501-6.[20]

Material properties	Values
Longitudianl modulus E_1 (GPa)	147
Transverse moduli $E_2 = E_3$ (GPa)	10.3
In-plane shear moduli $G_{12} = G_{13}$ (GPa)	7.0
Shear modulus G_{23} (GPa)	3.7
In-plane Poisson's ratios $v_{12} = v_{13}$	0.3
Poisson's ratio v_{23}	0.5
Longitudinal tensile strength X_T (MPa)	2280
Longitudinal compressive strength X_C (MPa)	1725
Transverse tensile strength Y_T (MPa)	57
Transverse compressive strength Y_C (MPa)	228
In-plane shear strength $S_{12} = S_{13}$ (MPa)	75

Table 2. Cohesive strength properties of AS4/3501-6.[21]

Material parameters	Values
Cohesive normal strength S_n (MPa)	60
Cohesive shear strengths $S_s = S_t$ (MPa)	68
Mode I G_{Ic} (N/mm)	0.075
Modes II and III $G_{IIc} = G_{IIIc}$ (N/mm)	0.547

adjacent plies. Each ply and cohesive layer thicknesses are 0.6 mm and 0.05 mm, respectively. An out-of-plane compressive load is applied in the middle of the top surface of the laminate, and both ends of the laminate are simply supported on the bottom surface (Figure 11). The initial delamination (pre-crack $a = 31.75$ mm) is located at the −45/0 interface near the right end part of the laminate (Figure 12). Under the compressive load, compressive normal stresses are generated in the cohesive elements at the interfaces. When cohesive elements fail and their material properties are degraded, the compressive normal stresses may result in interpenetration, leading to spurious results. This problem is overcome by assigning a very large value (e.g. 10^6 times of the original value) to the stiffness in the normal direction of the failed cohesive elements. This is, in effect, modeling the contact between plies in the laminate through a penalty method.

The failure patterns of the ENF laminate are shown in Figure 13 and are compared with experimental results. For simplicity and clarity, notations C1, C2, and C3 are used to denote the three ply cracks (−45°, 90°, and 45° plies); and D1, D2, and D3 are used to denote the three delaminations (90/−45, 45/90, and 0/45 interfaces), as shown in Figure 13. In the predicted failure patterns, the partitioned elements are used to model the cracks in plies and the failed cohesive elements are deleted to demonstrate delamination at interfaces. Generally, it can be seen from the comparison that the predicted patterns agree qualitatively with the experimental observations. It may be noted that the predicted D2 pattern is a rectangular shape (Figure 13(e)), which is different from that in experiment where it is indicated as a triangular shape (Figure 13(a)). However, the D2 pattern may not be clearly observed in the experiment because it may be partially hidden by the 45° ply on top of it.

When the load is increased, the pre-crack at the 0/−45 interface propagates in a straight front perpendicular to the fiber direction in the 0° ply. After a short propagation of the pre-crack, C1 and D1 occur first at edge 2 (the right edge as indicated in Figure 13(a)) and propagate simultaneously backward to the propagating direction of the pre-crack, as shown in Figure 14(a) and (b). After C1 is fully formed and D1 extends through the width, C2 occurs at edge 2 in the 90° ply and extends quickly through the width. Then D2 initiates and propagates forward with a straight front parallel to the fiber direction in the 90° ply, as shown in Figure 14(c) and (d). After C2 and D2 occurring and the load increased, C3 and D3 will occur at edge 2 and propagate forward, as shown in Figure 14(e) and (f). During this progression, D2 continuously propagates till C3 is fully formed (i.e. the 45° ply is fully cracked). After C3 is fully formed and D3 extends through the width, no more failures propagate and there are only 0° plies without failure below the symmetrical plane of the laminate. In summary, the failure progression sequence is that C1 and D1 occur and fully form; then C2 and D2 occur and are shortly followed by C3 and D3.

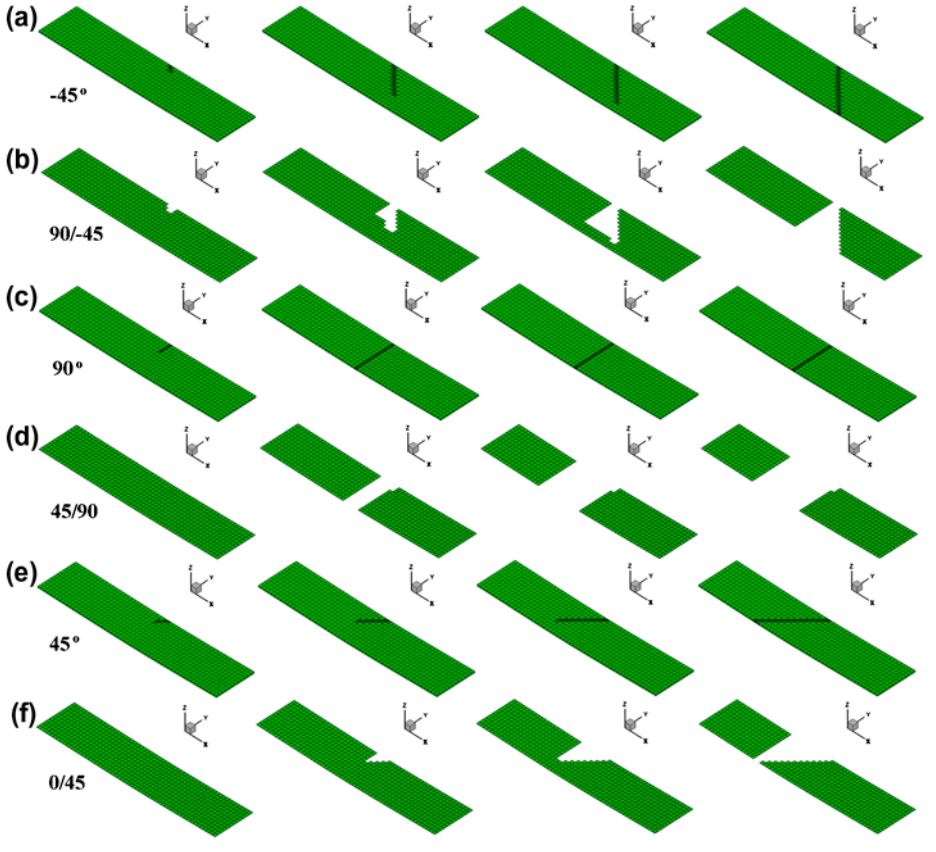

Figure 14. Failure progressions: (a) matrix crack in the −45° ply (C1), (b) delamination at the 90/−45 interface (D1), (c) matrix crack in the 90° ply (C2), (d) delamination at the 45/90 interface (D2), (e) matrix crack in the 45° ply (C3), and (f) delamination at the 0/45 interface (D3).

4. Conclusions

An XFEM-CE approach for modeling delamination and matrix crack interactions in composite laminates is presented in this paper. In this approach, matrix cracks are modeled by XFEM with the maximum stress criterion for determining crack initiation in matrix. Delaminations and their interactions with matrix cracks are modeled by cohesive elements with a zig-zag evolution model based on the traction–separation law. Enriched cohesive elements were also presented in the XFEM framework to better account for the interactions between delaminations and matrix cracks. Failure analyses of carbon/epoxy DCB and ENF laminates with layups $[0/90]_s$, $[0/45]_s$, and $[0/-45/90/45/0]_s$ were used to demonstrate the application of the proposed XFEM-CE approach in a qualitative manner. Progressive failures of the major matrix crack in plies and the extensive delamination at interfaces between plies were illustrated. The numerical results show that typical failure patterns in the DCB and ENF laminates were reasonably predicted by the XFEM-CE approach. This approach provides a potential numerical simulation tool for complex failures in composite structures.

Acknowledgements

This work was supported by National University of Singapore under the NUS Incentive Grant and Singapore A*STAR (Agency for Science, Technology and Research) through the MIMO (Materials Innovation for Marine & Offshore Applications) Project under Grant No. 1123004033.

References

[1] Tay TE. Characterization and analysis of delamination fracture in composites: an overview of developments from 1990 to 2001. App. Mech. Rev. 2003;56:1–32.
[2] Tay TE, Liu G, Tan VBC, Sun XS, Pham DC. Progressive failure analysis of composites. J. Compos. Mater. 2008;42:1921–1966.
[3] Moës N, Dolbow J, Belytschko T. A finite element method for crack growth without remeshing. Int. J. Numer. Meth. Eng. 1999;46:131–150.
[4] Sukumar N, Moës N, Moran B, Belytschko T. Extended finite element method for three-dimensional crack modelling. Int. J. Numer. Meth. Eng. 2000;48:1549–1570.
[5] Dolbow J, Moës N, Belytschko T. Discontinuous enrichment in finite elements with a partition of unity method. Finite Elem. Anal. Des. 2000;36:235–260.
[6] Huynh DBP, Belytschko T. The extended finite element method for fracture in composite materials. Int. J. Numer. Meth. Eng. 2009;77:214–239.
[7] Sun XS, Tan VBC, Liu G, Tay TE. An enriched element-failure method (REFM) for delamination analysis of composite structures. Int. J. Numer. Meth. Eng. 2009;79:639–666.
[8] Yang QD, Cox BN. Cohesive models for damage evolution in laminated composites. Int. J. Fracture. 2005;133:107–137.
[9] Cox JV. An extended finite element method with analytical enrichment for cohesive crack modeling. Int. J. Numer. Meth. Eng. 2009;78:48–83.
[10] Guiamatsia I, Ankersen JK, Davies GAO, Iannucci L. Decohesion finite element with enriched basis functions for delamination. Compos. Sci. Technol. 2009;69:2616–2624.
[11] Guiamatsia I, Davies GAO, Ankersen JK, Iannucci L. A framework for cohesive element enrichment. Compos. Struct. 2010;92:454–459.
[12] Samimi M, Van Dommelen JAW, Geers MGD. An enriched cohesive zone model for delamination in brittle interfaces. Int. J. Numer. Meth. Eng. 2009;80:609–630.
[13] Fang XJ, Yang QD, Cox BN, Zhou ZQ. An augmented cohesive zone element for arbitrary crack coalescence and bifurcation in heterogeneous materials. Int. J. Numer. Meth. Eng. 2011;88:841–861.
[14] Tay TE, Sun XS, Tan VBC. Towards an integrated XFEM-CE approach for the modeling of matrix cracks and delamination interactions. Proceedings of the 1st Brazilian Conference on Composite Materials (BCCM-1); 2012.
[15] Sun XS, Tan VBC, Tay TE. An integrated XFEM-CE approach for modeling matrix cracks and delamination interactions in composite laminates with angled plies. Proceedings of the 19th International Conference on Composite Materials (ICCM-19); 2013.
[16] de Berg M, van Kreveld M, Overmars M, Schwarzkopf O. Computational geometry. 2nd ed. Springer-Verlag; 2000.
[17] Soden PD, Hinton MJ, Kaddour AS. A comparison of the predictive capabilities of current failure theories for composite laminates. Compos. Sci. Technol. 1998;58:1225–1254.
[18] Hinton MJ, Kaddour AS. The background to the Second World-Wide Failure Exercise. J. Compos. Mater. 2012;46:2283–2294.
[19] Ridha M, Tan VBC, Tay TE. Traction–separation laws for progressive failure of bonded scarf repair of composite panel. Compos. Struct. 2011;93:1239–1245.
[20] Daniel IM. Engineering mechanics of composite materials. 2nd ed. New York: Oxford University Press; 2006.
[21] Dávila CG, Camanho PP. Analysis of the effects of residual strains and defects on skin/stiffener debonding using decohesion elements. Proceedings of the 44th AIAA/ASME/ASCE/AHS/ASC Structures, Structural Dynamics and Materials Conference, Paper No. AIAA-2003-1465.
[22] Tao J, Sun CT. Influence of ply orientation on delamination in composite laminates. J. Compos. Mater. 1998;32:1933–1947.